**Proceedings of HT2008**
**2008 ASME Summer Heat Transfer Conference**
**August 10-14, 2008, Jacksonville, Fl., USA**

# HT2008-56094

# DEVELOPMENT OF A FLOW REGIME MAP FOR A HORIZONTAL PIPE WITH THE MULTI-CLASSIFICATION SUPPORT VECTOR MACHINES

**L. M. Tam**
**Department of Electromechanical Engineering, Faculty of Science and Technology, and Institute for the Development and Quality, University of Macau, Av. Padre Tomás Pereira, Taipa, Macau, China.**
**fstlmt@umac.mo**

**A. J. Ghajar**
**School of Mechanical and Aerospace Engineering, Oklahoma State University, Stillwater, Oklahoma, USA.**
**afshin.ghajar@okstate.edu**

**H. K. Tam**
**Department of Electromechanical Engineering, Faculty of Science and Technology, University of Macau, Av. Padre Tomás Pereira, Taipa, Macau, China.**
**hktam@umac.mo**

**S. C. Tam**
**Department of Mathematics, Faculty of Science and Technology, University of Macau, Av. Padre Tomás Pereira, Taipa, Macau, China.**
**fstsct@umac.mo**

## ABSTRACT

For horizontal circular pipes under uniform wall heat flux boundary condition and three different inlet configurations (re-entrant, square-edged, bell-mouth), Ghajar and Tam (1995) developed flow regime maps for the determination of the boundary between single-phase forced and mixed convection using experimental data of Ghajar and Tam (1994). Based on the ratio of the local peripheral heat transfer coefficient at the top and the bottom, the heat transfer data was classified as either forced or mixed convection among the different flow regimes. The forced-mixed convection boundary was then obtained by empirical correlations. From the flow maps, heat transfer correlations for different flow regimes were recommended. Recently Trafalis et al. (2005) used the Multi-class Support Vector Machines (SVM) method to classify vertical and horizontal two-phase flow regimes in 4 pipes with good accuracy. In this study, the SVM method was applied to the single-phase experimental data of Ghajar and Tam (1994) and new flow regime maps were developed. Five flow regimes (forced turbulent, forced transition, mixed transition, forced laminar, mixed laminar) were identified in the flow maps using Reynolds and Rayleigh numbers as the identifying parameters. The flow regimes on the boundaries of the new maps were represented by the SVM decision functions. The results show that the new flow regime maps for the three types of inlets can classify the forced and mixed convection experimental data in different flow regimes with good accuracy.

## NOMENCLATURE

$c_p$ = specific heat at constant pressure, kJ/(kg-K)
D = inside diameter of the tube, m
g = acceleration of gravity, m/s$^2$
Gr = local bulk Grashof number (= $g\beta\rho^2D^3(T_w-T_b)/\mu_b^2$)
h= local peripheral heat transfer coefficient, W/(m$^2$-K)
$h_t$ = local peripheral heat transfer coefficient at the top of tube, W/(m$^2$-K)
$h_b$ = local peripheral heat transfer coefficient at the bottom of tube, W/(m$^2$-K)
j = Colburn j-factor (= $StPr^{0.67}$)
k = thermal conductivity, W/(m$^2$-K)
n = number of classes
Nu = local average or fully developed peripheral Nusselt number (= hD/k)
Pr = local bulk Prandtl number (= $c_p\mu_b/k$)
Ra = local bulk Rayleigh number (= GrPr)

Re = local bulk Reynolds number (= $\rho VD/\mu_b$)
St = Stanton number ( = Nu/Re Pr)
$T_b$ = local bulk temperature, ºC
$T_w$ = local wall temperature, ºC
V = average velocity in the test section, m/s
x = local distance along the test section from the inlet, m

**Greek symbols**
$\beta$ = coefficient of thermal expansion, $K^{-1}$
$\mu_b$ = local bulk dynamic viscosity, Pa-s
$\mu_w$ = local wall dynamic viscosity, Pa-s
$\rho$ = local bulk density, $kg/m^3$

## INTRODUCTION

In a horizontal pipe, the secondary flow is produced by heating the fluid through the pipe wall. The fluid near the heated pipe wall, due to its higher temperature and lower density, circulates upward, while the fluid near the central region of the pipe, having a lower temperature and a higher density, circulates downward. These counter-rotating transverse vortices that are superimposed on the streamwise main flow due to free convection effects (buoyancy influences) can significantly increase the forced convection heat transfer. The magnitude of heat transfer coefficient in combined (or mixed) convection can obviously be different from those in both pure free and forced convection. For the design purpose, it is of interest to know when the free convection effect can be neglected and when they have to be accounted for. Metais and Eckert (1964) recommended the use of the flow regime map of Figure 1 for determining the boundary between mixed and forced convection in horizontal pipes under uniform wall temperature boundary conditions. For the identified pure forced or mixed convection heat transfer regime, a heat transfer correlation for the laminar or turbulent flow is offered on the map. In Figure 1, the flow regime boundary was arbitrarily determined to be the location where the mixed convection heat transfer does not deviate by more than 10% from pure forced flow represented by a given Reynolds number. The value of the parameter GrPrD/x indicates whether it is necessary to consider buoyancy effects. The shaded area of Figure 1 is the transition region. Based on the experimental results of Kern and Othmer (1943), Metais (1963) determined the transition Reynolds number range to be between 600 and 800. The transition Reynolds number range between laminar and turbulent forced convection from the figure appears to be between 2000 and 3100. However, Metais (1963) did not report the source of this information.

Ghajar and Tam (1995) have applied the flow regime map given in Figure 1 to the laminar-transitional-turbulent forced and mixed convection experimental data of Ghajar and Tam (1994) obtained in a horizontal pipe with uniform wall heat flux and three different inlet configurations. As shown in Figure 2, excluding all the forced turbulent convection data, the experimental data for forced laminar, mixed laminar, mixed transition, and forced transition were not predicted correctly. The reason for this discrepancy is mainly due to the influence of boundary condition and inlet geometry. To properly account for these influences, Ghajar and Tam (1995) developed their own flow regime map as shown in Figure 3. As detailed in Ghajar and Tam (1995), the flow regime map given in Figure 3 was verified with Ghajar and Tam's (1994) experimental data and the flow regime map correctly predicted the experimental data in the different flow regimes for each inlet configuration.

In a recent study, Trafalis et al. (2005) used the Multi-class Support Vector Machines (SVM) method to classify vertical and horizontal two-phase flow regimes in four different pipes. The predictions from SVM method was shown to be more accurate than predictions based on empirical correlations. This is a new approach for the flow regime classification and up to now has not been used to classify single-phase forced-mixed convection in horizontal pipes. The main objective of this study is to apply the SVM method to classify single-phase heat transfer data and develop new flow regime maps. For this purpose the single-phase forced and mixed convection experimental data of Ghajar and Tam (1994) obtained in a horizontal pipe with three different inlet configurations under uniform wall heat flux boundary condition was used.

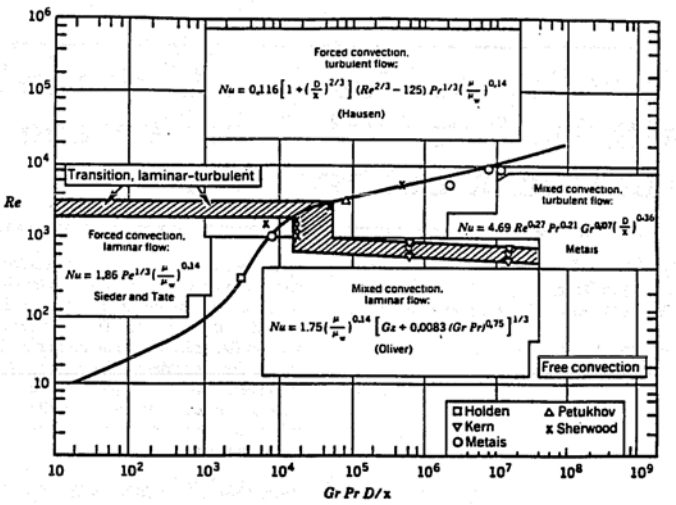


Figure 1: Free, forced, and mixed convection regimes for flow in horizontal circular tubes for $10^{-2}$ < Pr D/x < 1 and uniform wall temperature boundary condition, taken from Aung (1987).

## EXPERIMENTAL DATASET

The heat transfer experimental data used in this study, along with a detailed description of the experimental apparatus and procedures used, were reported by Ghajar and Tam (1994). A schematic of the overall experimental setup used for heat transfer measurements is shown in Figure 4. In this paper, only a brief description of the experimental setup and procedures will be provided. The local forced and mixed convective measurements were made in a horizontal, electrically heated, stainless steel circular straight tube under uniform wall heat flux boundary condition and three types of inlet

configurations(re-entrant, square-edged, and bell-mouth), as shown in Figure 5.

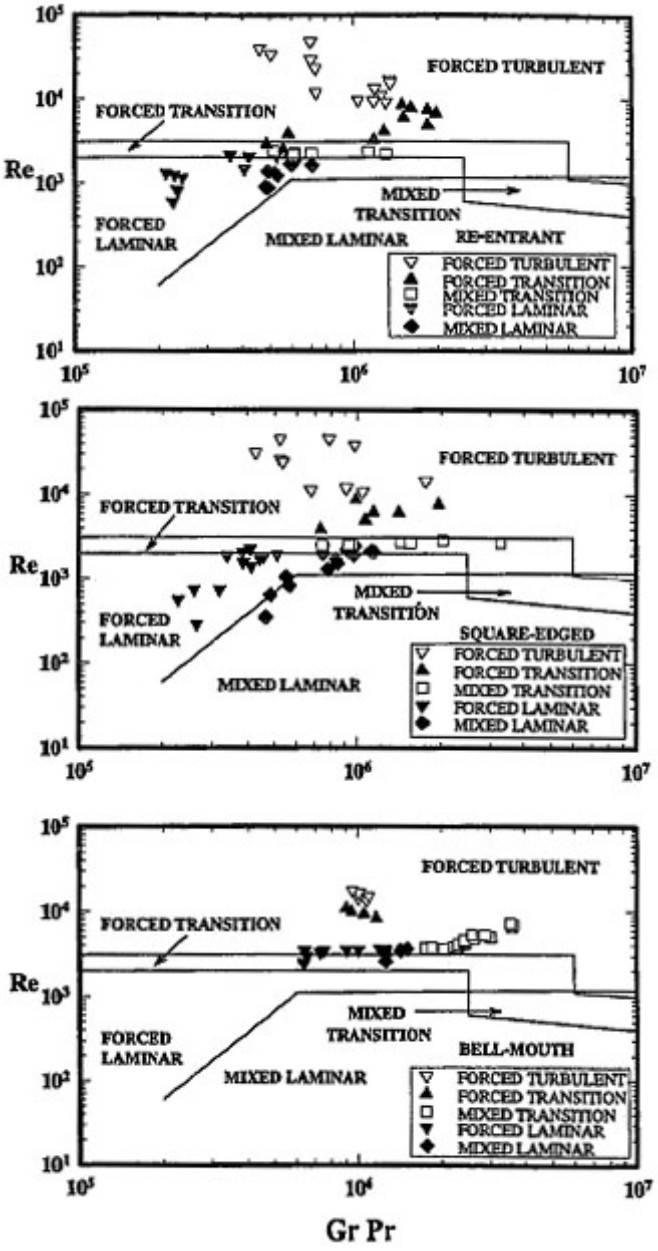


Figure 2: Comparison of Metais and Eckert's (1964) flow regime map with experimental data (Ghajar and Tam, 1994) for uniform wall heat flux boundary condition and three different inlet configurations, taken from Ghajar and Tam (1995).

The pipe had an inside diameter of 1.58 cm and an outside diameter of 1.90 cm. The total length of the test section was 6.10 m, providing a maximum length-to-diameter ratio of 385.

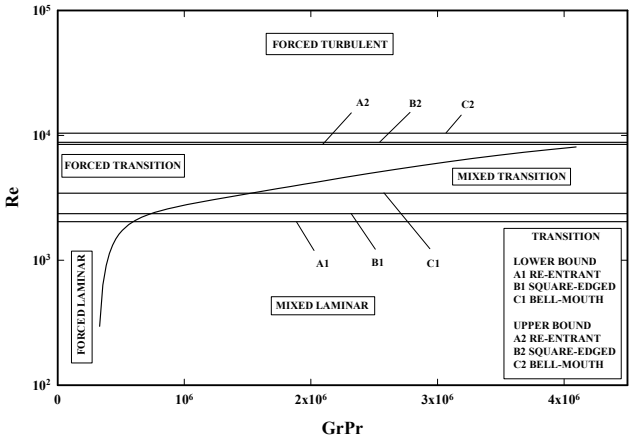


Figure 3: The flow regime map for forced and mixed convection flow in horizontal circular tubes with three different inlet configurations and uniform wall heat flux boundary condition, taken from Ghajar and Tam (1995).

A uniform wall heat flux boundary condition was maintained by a dc arc welder. Thermocouples (T-type) were placed on the outer surface of the tube wall at close intervals near the entrance and at greater intervals further downstream. Twenty-six axial locations were designated, with four thermocouples placed at each location. The thermocouples were placed 90 degrees apart around the periphery. From the local peripheral wall temperature measurements at each axial location, the inside wall temperatures and the local heat transfer coefficients were calculated (Ghajar and Kim, 2006). In these calculations, the axial conduction was assumed negligible (RePr > 4,200 in all cases), but peripheral and radial conduction of heat in the tube wall were included. In addition, the bulk fluid temperature was assumed to increase linearly from the inlet to the outlet. As reported by Ghajar and Tam (1994), the uncertainty analyses of the overall experimental procedures showed that there is a maximum of 9% uncertainty for the heat transfer coefficient calculations. Moreover, the heat balance error for each experimental run indicated that in general, the heat balance error was less than 5%. For Reynolds numbers lower than 2500 where the flow was strongly influenced by secondary flow, the heat balance error was slightly higher (5–8%) for that particular Reynolds number range. To ensure a uniform velocity distribution in the test fluid before it entered the test section, the flow passed through calming and inlet sections. The calming section had a total length of 61.6 cm and consisted of a 17.8 cm diameter acrylic cylinder with three perforated acrylic plates, followed by tightly packed soda straws sandwiched between galvanized steel mesh screens.

Before entering the inlet section, the test fluid passed through a fine mesh screen and flowed undisturbed through 23.5 cm of a 6.5 cm-diameter acrylic tube before it entered the test section. The inlet section had the versatility of being modified to incorporate a re-entrant or bell-mouth inlet (see Figure 5). The re-entrant inlet was simulated by sliding 1.93 cm of the tube entrance length into the inlet section, which was otherwise the square-edged (sudden contraction) inlet. For the bell-mouth inlet, a fiberglass nozzle with a contraction ratio of 10.7 and a total length of 23.5 cm was used in place of the inlet section. In the experiments, distilled water and mixtures of distilled water and ethylene glycol were used. They collected 2149 experimental data points from laminar to turbulent flow for the three inlets (see Tam, 1995), and their experiments covered a local bulk Reynolds number range of 280 to 49000, a local bulk Prandtl number range of 4 to 158, a local bulk Grashof number range of 1000 to $2.5\times10^5$, and a local bulk Nusselt number range of 13 to 258. The wall heat flux for their experiments ranged from 4 to 670 kW/m$^2$.

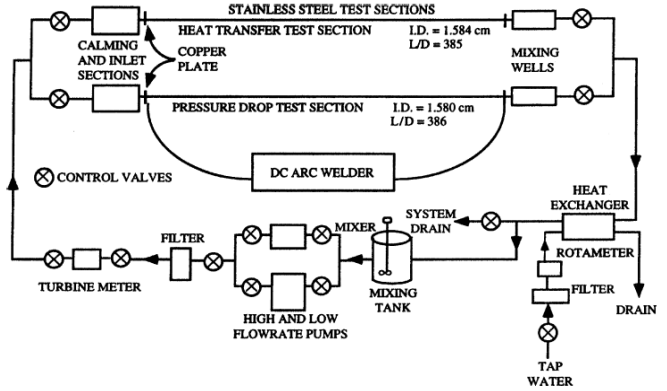


Figure 4: Schematic diagram of experimental setup.

## HEAT TRANSFER BEHAVIOR AND FLOW REGIME MAP OF GHAJAR AND TAM (1995)

As seen in Figure 6 (Ghajar and Tam, 1994), the abrupt change of heat transfer characteristic in the transition region is obvious. In this region, the flow has both laminar and turbulent characteristics. As shown in Figure 6, the beginning and end of the transition region is inlet configuration dependent. In addition, these transition Reynolds number limits are x/D-dependent. To determine the range of heat transfer transition Reynolds number ($3 \le x/D \le 192$), Ghajar and Tam (1995) used their experimental data and developed figures similar to Figure 6 for 20 other x/D locations. From these figures, the heat transfer transition Reynolds number range for each inlet was determined to be about 2000-8500 for the re-entrant inlet, 2400-8800 for the square-edged inlet, and 3400-10,500 for the bell-mouth inlet.

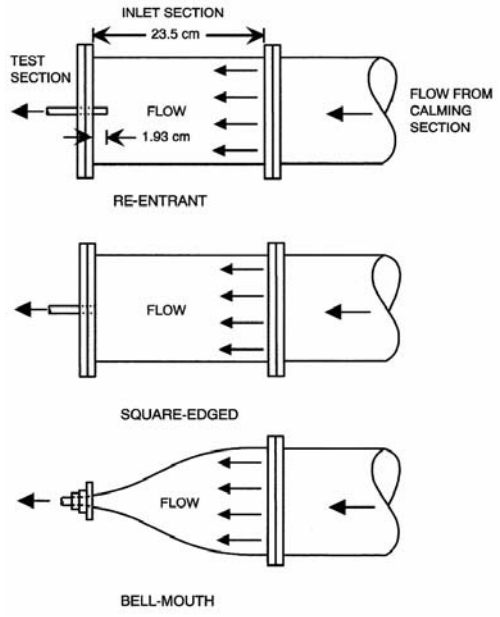


Figure 5: Schematic of the three different inlet configurations.

The application of heat to the tube wall produces a temperature difference in the fluid. The fluid near the tube wall has a higher temperature and lower density than the fluid close to the centerline of the tube. This temperature difference may produce a secondary flow due to free convection.

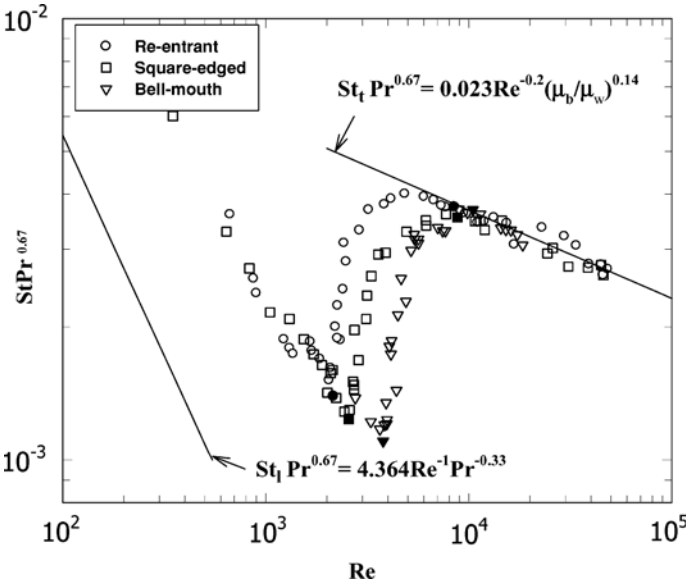


Figure 6: Heat transfer in the transition region at x/D = 192 (solid symbols designate the start and end of the transition region for each inlet), taken from Ghajar and Tam (1994).

In the laminar flow region, the effect of free convection (or buoyancy) on forced convection can be clearly seen in Figure 6, which resulted in an upward parallel shift of the Colburn j factors from their fully developed forced convection laminar values. In the transition region, the effect of mixed convection cannot be easily seen unless the local heat transfer information, which is the ratio of the local peripheral heat transfer coefficient at the top of the tube to the local peripheral heat transfer coefficient at the bottom of the tube ($h_t/h_b$), is carefully examined. To properly account for the effect of mixed convection, Ghajar and his coworkers (1994, 1995, 1998) used four thermocouples around the periphery of the tube (90° apart) at each of the twenty-six designated axial locations along the tube. The thermocouples were at close intervals near the entrance of the tube and at greater intervals further downstream. According to Ghajar and Tam (1994, 1995), $h_t/h_b$ should be close to unity (0.8–1.0) for forced convection and is much less than unity (< 0.8) for a case in which mixed convection exists. Figure 7 (from Tam and Ghajar, 2006) shows the effect of secondary flow on heat transfer coefficient for different inlets and flow regimes. For the re-entrant, square-edged, and bell-mouth inlets, when the Reynolds numbers were greater than 2500, 3000, and 8000, respectively, the flows were dominated by forced convection heat transfer, and the heat transfer coefficient ratios ($h_t/h_b$) did not fall below 0.8–0.9. (In fact, at times they exceeded unity due to the roundoff errors in the property evaluation subroutine of the data reduction program, Ghajar and Kim, 2006.) The flows dominated by mixed convection heat transfer had $h_t/h_b$ ratios beginning near 1 but dropped off rapidly as the length-to-diameter ratio (x/D) increased. Beyond about 125 diameters from the entrance, the ratio was almost invariant with x/D, indicating a much less dominant role for forced convection heat transfer and increased free convection activity. In reference to Figure 7, it is interesting to observe that the starting length necessary for the establishment of the free convection effect for low Reynolds number flows is also inlet-dependent. When the secondary flow is established, a sharp decrease in $h_t/h_b$ occurs. Depending on the type of inlet configuration, for low Reynolds number flows (Re < 2500 for re-entrant, < 3000 for square-edged, and < 8000 for bell-mouth), the flow can be considered to be dominated by forced convection over the first 20–70 diameters from the entrance to the tube.

It was shown in Figure 2 that the flow regime map developed by Metais and Eckert (1964) is not suitable for the uniform wall heat flux boundary condition, and Ghajar and Tam (1995) developed their own flow regime map as shown in Figure 3. In Figure 3, the laminar-transition-turbulent lines were determined from the transition Reynolds number limits shown in Figure 2. For each axial location ($3 \le x/D \le 192$), the laminar-transition and the transition-turbulent lines were adjusted upward or downward depending on the x/D value. Comparing with the Metais and Eckert's (1964) flow regime map, the boundary between forced and mixed convection regions in the Ghajar and Tam's (1995) flow regime map is more reasonable and reliable because the former was arbitrarily determined and the latter was obtained from the ratio of the local peripheral heat transfer coefficient at the top of the tube to the local peripheral heat transfer coefficient at the bottom of the tube ($h_t/h_b$).

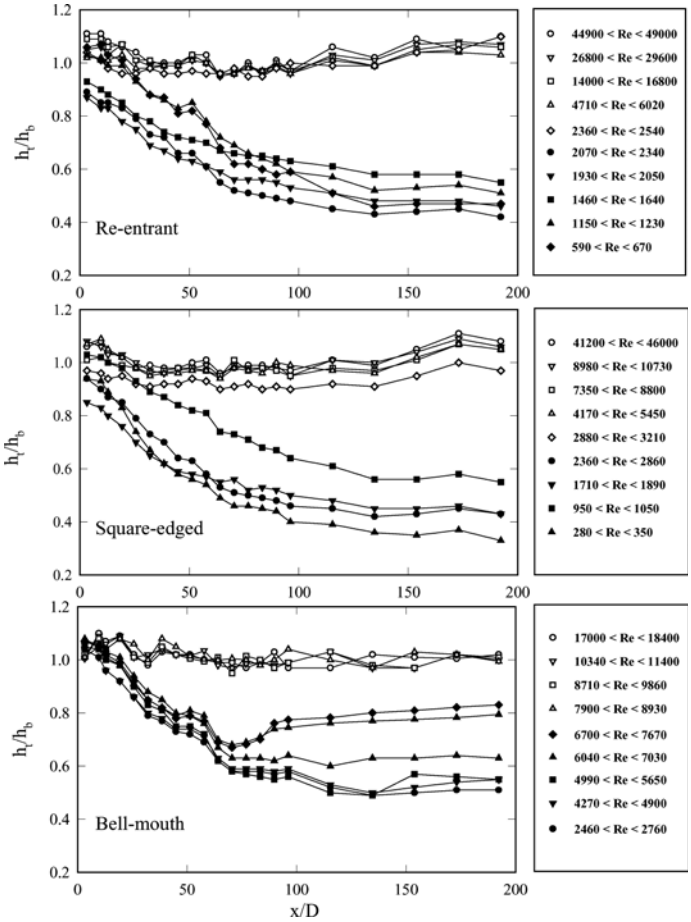

Figure 7: Effect of secondary flow on heat transfer coefficient for different inlets and flow regimes, taken from Tam and Ghajar (2006).

To show further details about the flow regime map of Ghajar and Tam (1995), a total of 2149 experimental data points taken from Ghajar and Tam (1994) and Tam (1995) for the three different inlet configurations were classified based on different flow regimes and different types of convection. Table 1 summarizes the results of the classification and the percent accuracy of predictions by the flow regime map of Ghajar and Tam (1995). Figure 8 shows the results on the flow regime map. The transition lines shown on the figure are based on x/D = 192. Figure 8 clearly shows that overall the data points were correctly arranged in the flow regime map. However, the prediction of the flow regime boundaries can be further improved. For this purpose the SVM method will be explored.

Table 1: Classification of the experimental data by using the transition Reynolds number limits and the heat transfer coefficient ratios ($h_t/h_b \geq 0.8$ or $< 0.8$)

| Type of Inlet | Flow Regime | Type of Convection | No. of Data Points | Accuracy by using the Flow Regime Map of Ghajar and Tam (1995) |
|---|---|---|---|---|
| Re-entrant (806 pts.) | Laminar | Forced ($h_t/h_b \geq 0.8$) | 47 | 44 data points (93.6%) |
| | | Mixed ($h_t/h_b < 0.8$) | 145 | 79 data points (54.5%) |
| | Transition | Forced ($h_t/h_b \geq 0.8$) | 314 | 295 data points (93.9%) |
| | | Mixed ($h_t/h_b < 0.8$) | 50 | 23 data points (46.0%) |
| | Turbulent | Forced ($h_t/h_b \geq 0.8$) | 250 | 250 data points (100.0%) |
| | **Overall** | **Forced & Mixed** | **806** | 691 data points **(85.7%)** |
| Square-edged (750 pts.) | Laminar | Forced ($h_t/h_b \geq 0.8$) | 80 | 48 data points (60.0%) |
| | | Mixed ($h_t/h_b < 0.8$) | 227 | 195 data points (85.9%) |
| | Transition | Forced ($h_t/h_b \geq 0.8$) | 124 | 120 data points (96.8%) |
| | | Mixed ($h_t/h_b < 0.8$) | 91 | 67 data points (73.6%) |
| | Turbulent | Forced ($h_t/h_b \geq 0.8$) | 228 | 228 data points (100.0%) |
| | **Overall** | **Forced & Mixed** | **750** | 658 data points **(87.7%)** |
| Bell-mouth (593 pts.) | Laminar | Forced ($h_t/h_b \geq 0.8$) | 34 | 31 data points (91.2%) |
| | | Mixed ($h_t/h_b < 0.8$) | 72 | 25 data points (34.7%) |
| | Transition | Forced ($h_t/h_b \geq 0.8$) | 168 | 154 data points (91.7%) |
| | | Mixed ($h_t/h_b < 0.8$) | 189 | 165 data points (87.3%) |
| | Turbulent | Forced ($h_t/h_b \geq 0.8$) | 130 | 130 data points (100.0%) |
| | **Overall** | **Forced & Mixed** | **593** | 505 data points **(85.2%)** |

## THE SUPPORT VECTOR MACHINES FOR BINARY CLASSIFICATION

In this section, the SVM algorithm for classification will be introduced. First of all, the two-class classification is considered. The following material is based on the work of Vapnik (1995) and Schölkopf and Smola (2002). Suppose the training data of two classes

$$(\mathbf{x}_1, y_1), \ldots, (\mathbf{x}_m, y_m), \mathbf{x}_i \in \mathbf{R}^d, y_i \in \{+1, -1\}, i = 1, \ldots, m$$

where $\mathbf{R}^d$ is the d-dimensional Euclidian space and m is the number of training data. A hyperplane in $\mathbf{R}^d$ (Vapnik, 1979) is a set $\{\mathbf{x} \mid < \mathbf{w}, \mathbf{x} > + b = 0\}$ where $\mathbf{w}$ is d-dimensional vector, $b \in \mathbf{R}$ and <**w**, **x**> is the dot product in $\mathbf{R}^d$ .For simplicity, it also can be represented by (**w**, b).

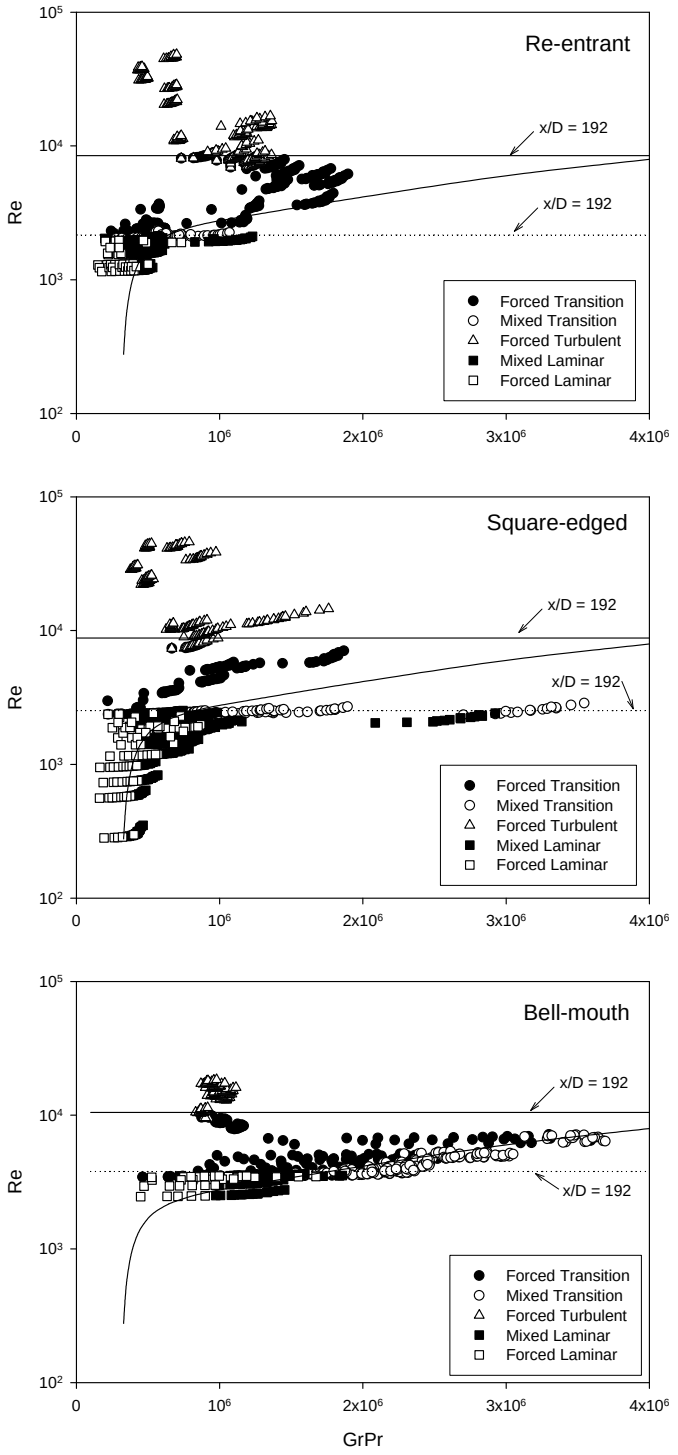


Figure 8: Comparison of flow regime map of Ghajar and Tam (1995) with the experimental data (Ghajar and Tam, 1994; Tam, 1995) for uniform wall heat flux boundary condition and three different inlet configurations.

A separating hyperplane (**w**, b) with respect to the data set $(\mathbf{x}_1, y_1), \ldots, (\mathbf{x}_m, y_m)$ if

$$\text{sgn}(< \mathbf{w}, \mathbf{x}_k > + \text{b}) = \text{y}_k, k = 1, ..., m \quad (1)$$

Furthermore, it is called canonical if it is scaled such that

$$\min_{i=1,...,m} |< \mathbf{w}, \mathbf{x}_i > + b| = 1, \quad (2)$$

Hence, the canonical form (**w**, b) of a separating hyperplane is unique and the distance of the point closet to the hyperplane is now equal to $1/\|\mathbf{w}\|$. Therefore, only the canonical forms of separating hyperplanes are considered in this paper.

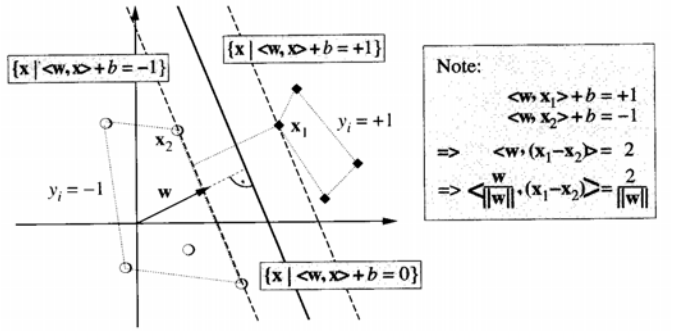


Figure 9: Schematic diagram shows the separating hyperplanes between the two-class training data, taken from Schölkopf and Smola (2002).

The separating hyperplane with canonical form (**w'**, b') which has the least classification risk should have the biggest value $1/\|\mathbf{w}'\|$ (see Vapnik, 1995). Therefore, the following problem can be constructed to solve **w'**:

$$\min_{\mathbf{w} \in R^d, \text{b} \in \text{R}} \quad \tau(\mathbf{w}) = \frac{1}{2}\|\mathbf{w}\|^2 \quad (3)$$

$$\text{subject to} \quad \text{y}_i(< \mathbf{x}_i, \mathbf{w} > + \text{b}) \geq 1 \text{ for all } \text{i} = 1, \ldots, \text{m}. \quad (4)$$

This problem is a constraint primal optimization problem. Usually, it is solved by the convex optimization method (see Boyd and Vandenberghe, 2004). The dual problem can be written in the Lagrangian form,

$$L(\mathbf{w}, b, \boldsymbol{\alpha}) = \frac{1}{2}\|\mathbf{w}\|^2 - \sum_{i=1}^{m} \alpha_i(\text{y}_i(< \mathbf{x}_i, \mathbf{w} > + \text{b}) - 1), \quad (5)$$

with Lagrange multipliers $\alpha_i \geq 0$. To minimize Eq. (3), the saddle point of Eq. (5) has to be solved. It means to minimize over the primal variables **w** and b and maximize over the dual variables $\alpha_i$. The partial derivatives of L with respect to the primal variables equal to zero yields the two equations

$$\frac{\partial}{\partial b} L(\mathbf{w}, b, \boldsymbol{\alpha}) = 0, \frac{\partial}{\partial \mathbf{w}} L(\mathbf{w}, b, \boldsymbol{\alpha}) = 0, \quad (6)$$

which leads to

$$\sum_{i=1}^{m} \alpha_i y_i = 0, \quad (7)$$

and

$$\mathbf{w} = \sum_{i=1}^{m} \alpha_i y_i \mathbf{x}_i. \quad (8)$$

According to the Karush-Kuhn-Tucker (KKT) theorem (see Boyd and Vandenberghe, 2004), only the Lagrange multipliers $\alpha_i$ that are non-zero at the saddle point, correspond to constraints of Eq. (4) which are precisely met. Formally, for all i=1,…,m,

$$\alpha_i[\text{y}_i(< \mathbf{x}_i, \mathbf{w} > + \text{b}) - 1] = 0 \quad (9)$$

The patterns $\mathbf{x}_i$ for which $\alpha_i > 0$ are called Support Vectors. From Eq. (9), the support vectors lie exactly on the margin.

To solve the optimization problem, Eqs. (7) and (8) are substituted into the Lagrangian (Eq. (5)). Then, the dual form of the optimization problem is obtained:

$$\underset{\boldsymbol{\alpha} \in R^m}{\text{maximize}} \quad \text{W}(\boldsymbol{\alpha}) = \sum_{i=1}^{m} \alpha_i - \frac{1}{2}\sum_{i,j=1}^{m} \alpha_i \alpha_j \text{y}_i \text{y}_j < \mathbf{x}_i, \mathbf{x}_j >, \quad (10)$$

$$\text{subject to} \quad \alpha_i \geq 0, \quad \text{i} = 1, \ldots, \text{m}, \quad (11)$$

$$\text{and} \sum_{i=1}^{m} \alpha_i y_i = 0, \quad (12)$$

On substitution of the Eq. (8) into the decision function Eq. (1), the decision function in terms of dot products and the support vectors becomes

$$f(\mathbf{x}) = \text{sgn}\left(\sum_{i=1}^{m} \alpha_i y_i < \mathbf{x}, \mathbf{x}_i > + b)\right). \quad (13)$$

In fact, the foregoing algorithm can solely be applied to linear separable case. For the nonlinear input data, the nonlinear decision surface should be constructed. For constructing the nonlinear decision surface, kernels are used to transform the input data $x_1, \ldots, x_m \in \mathbf{R}^{\text{n}}$ ($\mathbf{R}^{\text{n}}$ is the input domain) into a high-dimensional feature space $\mathbf{R}^{\text{d}}$, using a map $\Phi : x_i \mapsto \mathbf{x}_{\text{i}}$ (see Figure 10). The patterns $\mathbf{x}_{\text{i}}$ shown previously equal to the results of mapping the original input patterns $\text{x}_{\text{i}}$ into a high-dimensional feature space, i.e., $\mathbf{x}_{\text{i}}$ equal to $\boldsymbol{\Phi}(x_i)$. The computation of dot product can be represented by a positive definite kernel k, such that

$$< \boldsymbol{\Phi}(x), \boldsymbol{\Phi}(x_i) >= k(x, x_i), \quad (14)$$

Normally, the polynomial, Gaussian, and tanh activation functions will be used as the kernel function. Then, the kernel trick leads the dual function, Eq. (10), and the decision function, Eq. (13), to be

$$\underset{\boldsymbol{\alpha} \in R^m}{\text{maximize}} \quad \text{W}(\boldsymbol{\alpha}) = \sum_{i=1}^{m} \alpha_i - \frac{1}{2}\sum_{i,j=1}^{m} \alpha_i \alpha_j \text{y}_i \text{y}_j k(\mathbf{x}_i, \mathbf{x}_j), \quad (15)$$

and

$$f(x) = \mathrm{sgn}\left(\sum_{i=1}^{m} \alpha_i \, y_i k(x, x_i) + b\right). \quad (16)$$

The constraint function of Eq. (3) is inadequate for practical problems. If an individual outlier in a data set, for instance a pattern which is mislabeled, can affect the construction of the hyperplane. Therefore, Cortes and Vapnik (1995) introduced an approach to alleviate this problem. The key point is to add the slack variables,

$$\xi_i \geq 0, \quad \text{where } i = 1, \ldots, m, \quad (17)$$

into the Eq. (4) to relax the separation constraints,

$$y_i (< \mathbf{x}_i, \mathbf{w} > + b) \geq 1 - \xi_i, \quad i = 1, \ldots, m. \quad (18)$$

If the $\xi_i$ is large enough, the constraint on ($\mathbf{x}_i$, $y_i$) can always be met. However, a very large value may affect the generalization for the unseen data. In order not to obtain the trivial solution where all $\xi_i$ take on large values, we thus need to penalize them in the objective function. Therefore, the objective function Eq. (3) and the constraint Eq. (4) are modified to the so-called C-SVC (C-Support Vector Classification):

$$\min_{\mathbf{w} \in N, \xi \in R} \tau(\mathbf{w}, \boldsymbol{\xi}) = \frac{1}{2}\|\mathbf{w}\|^2 + \frac{C}{m}\sum_{i=1}^{m} \xi_i, \quad (19)$$

$$\text{subject to } y_i (< \mathbf{x}_i, \mathbf{w} > + b) \geq 1 - \xi_i, \quad i = 1, \ldots, m. \quad (20)$$

$$\text{and } \xi_i \geq 0, \quad \text{where } i = 1, \ldots, m, \quad (21)$$

where the positive constant C can control the trade-off between minimizing the training error and maximizing the fraction of margin errors. It needs to be determined prior to the training. The C-SVC will be used in this study. Although the primal problem is changed, the decision function for C-SVC is also equal to Eq. (16).

Similar to Eqs. (10)-(12), the dual form of the C-SVC is shown below:

$$\underset{\boldsymbol{\alpha} \in R^m}{\text{maximize}} \quad W(\boldsymbol{\alpha}) = \sum_{i=1}^{m} \alpha_i - \frac{1}{2}\sum_{i,j=1}^{m} \alpha_i \alpha_j y_i y_j < \mathbf{x}_i, \mathbf{x}_j >, \quad (22)$$

$$\text{subject to } 0 \leq \alpha_i \geq \frac{C}{m}, \quad \text{for } i = 1, \ldots, m, \quad (23)$$

$$\text{and} \sum_{i=1}^{m} \alpha_i y_i = 0, \quad (24)$$

For computing the decision function (Eq. (16)), the coefficients $\alpha_i$ can be obtained by solving the above quadratic programming problem (Eqs. (22)-(24)). Besides, the threshold b can be obtained by averaging

$$b = y_j - \sum_{i=1}^{m} y_i \alpha_i k(y_j, y_i), \quad (25)$$

which is deduced from Eq. (9)

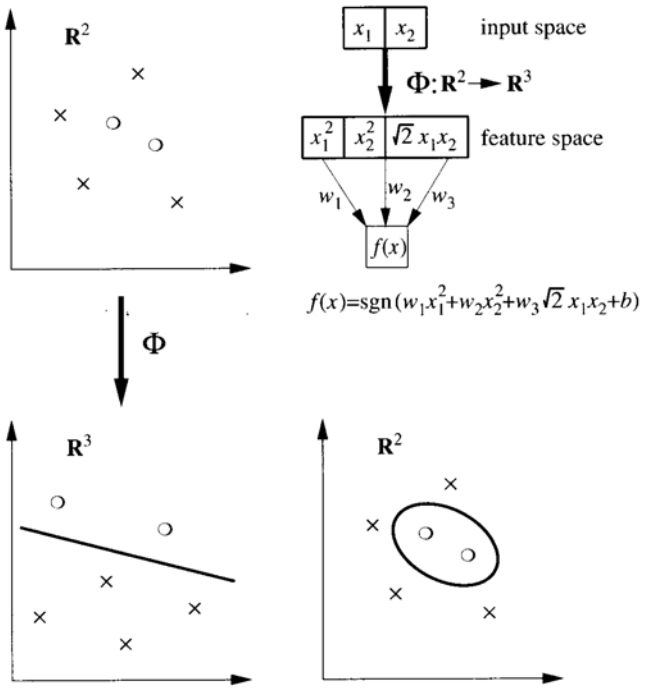


Figure 10: The 'kernelizing' process shows that the nonlinear input data (the input domain, $R^2$) is transformed to a higher-dimensional feature space $R^3$ and finally the nonlinear separating hyperplane is constructed in the input space, taken from Schölkopf and Smola (2002).

## THE MULTI-CLASS SVM

In the practical applications, the class labels $y_i$ always exceed two values, ±1. The binary-class SVM is not sufficient for classifying those problems. Therefore, the Multi-class SVM is developed for the multi-class problems. Hsu and Lin (2002) compared several Multi-class SVM methods, which are "one-against-all", "one-against-one", and DAGSVM. In that study, the "one-against-one" and DAGSVM methods were concluded to be more suitable for the practical applications than the other ones. Besides, Trafalis et al. (2005) also applied the "one-against-one" method for the multi-class problem successfully. Therefore, it is worth to apply the "one-against-one" method for the multi-class problem.

The "one-against-one" method was introduced by Knerr et al. (1990). The n(n-1)/2 classifiers (where n is the number of classes) are constructed and each classifier $P^{ij}$ is trained from two different classes where i and j denote the ith and jth classes. For example, 3 classes are needed to be identified by Multi-class SVM. Then, the 3 classifiers, namely $P^{12}$, $P^{13}$, and $P^{23}$, are constructed. When the classifier $P^{12}$ is trained, all the data points from class 1 are labeled with +1 and all the points from class 2 are labeled with -1; Similarly, for $P^{13}$, the points from class 1 are labeled with +1 and those from class 3 are labeled with -1; for $P^{23}$, the points from class 2 are labeled with +1 and those from class 3 are labeled with -1. For each training,

the binary classification problem (cf Eqs. (19)-(21)) for the particular two classes can be written as:

$$\min_{\mathbf{w}^{ij},b^{ij},\xi^{ij}} \quad \frac{1}{2}\left\|\mathbf{w}^{ij}\right\|^2 + C\sum_t \xi_t^{ij} \tag{26}$$

$$\text{subject to} \quad y_t(<\mathbf{x}_t, \mathbf{w}^{ij}> + b^{ij}) \geq 1 - \xi_t^{ij}, \text{ if } y_t = i, \tag{27}$$

$$y_t(<\mathbf{x}_t, \mathbf{w}^{ij}> + b^{ij}) \leq 1 + \xi_t^{ij}, \text{if } y_t = j, \tag{28}$$

$$\xi_t^{ij} \geq 0.$$

After solving the above primal problem for the particular two classes, the corresponding decision functions can be found. After the training, Friedman (1996) suggested to apply the voting strategy for the testing of the unseen data points. The voting approach is also called "Max Wins" strategy. The mechanism is: If the test sample $x$ is found in the i[th] class by the decision function, $f(x) = \text{sgn}\left(\sum_t \alpha_t^{ij} y_t k(x, x_t) + b^{ij}\right)$, the vote for the i[th] class is added by one. Otherwise, the vote for the j[th] class is increased by one. Then, the sample is evaluated by the other decision functions. After the full testing, the class with the largest vote is labeled to the sample. In the case that two classes have the identical votes, the one with the smallest class index is selected.

## RESULTS AND DISCUSSION

To develop the multi-class SVM model, the number of attributes (or input variables) and the number of classes is necessary to be considered first. From the flow regime map developed by Ghajar and Tam (1995), the two variables, GrPr and Re, are defined as the attributes. There are 5 classes outlined in the traditional flow map. The labels for the corresponding classes are: Class 1: forced laminar, Class 2: mixed laminar, Class 3: mixed transition, Class 4: forced transition, Class 5: forced turbulent. In this study, 80% of the experimental data (denoted by $M_a$) for each inlet were used to develop the model. The rest of the data (i.e., 20%, as denoted by $M_b$) were used for verification.

In this study, the C-SVC primal problem (Eqs. (19)-(21)) with the "one-against-one" method (Eqs. (26)-(28)) is used to develop the multi-class SVM model. The simple polynomial kernel $k(x, x_i) = (x_i^T x)^d$ is selected as the kernel function. Prior to the training, the constant, C, of Eq. (19) and the kernel parameter, *d*, are needed to be determined intuitively. After training the SVM model with the training data ($M_a$) and the combinations of C and *d* (the ranges of C and *d* are $[2^2,\ldots,2^{14}]$ and $[1,\ldots,3]$), the optimum values of these parameters for each inlet are determined according to the most accurate classification of the total data points (M). With the optimum values of the parameters (see Table 2), the accuracy of the classification of the heat transfer data for each inlet configuration using SVM model is represented in Tables 3-5. Based on the data for each inlet, three new flow regime maps with regime boundaries were developed as shown in Figures 11-13. The figures also show the five identified regions. Regarding to the accuracy of the new flow maps based on the SVM method, as seen in Tables 3-5, majority of the data points (almost 88%) were identified in the correct classes. 701 of the 806 re-entrant data points (87%), 658 of the 750 square-edged data points (88%), and 519 of the 593 data points (88%), were classified in the 5 pre-defined classes correctly. Compared to the results from Ghajar and Tam's (1995) flow regime map (Table 1), the SVM based flow regime map provided better overall accuracy. Figures 14-16, show the decision functions for separating the binary classes and the comparison between the SVM based flow regime maps and experimental data for the three inlets. The figures clearly show that the experimental data points are accurately classified by the new flow regime maps.

Table 2: The optimum values of C and d for developing the SVM models

| Models | C | *d* |
|---|---|---|
| Re-entrant model | 16 | 2 |
| Square-edged model | 4 | 2 |
| Bell-mouth model | 4096 | 2 |

Table 3: Accuracy of the proposed SVM model based on the re-entrant training data

| | Re-entrant Inlet<br>M – total points, $M_a$ – 80% training data, $M_b$ – 20% testing data | | |
|---|---|---|---|
| | No. of Data Points | Pts. Identified by SVM | % Accuracy |
| M | 806 | 701 | 86.9 |
| $M_a$ | 645 | 563 | 87.3 |
| $M_b$ | 161 | 138 | 85.7 |

Table 4: Accuracy of the proposed SVM model based on the square-edged training data

| | Square-edged Inlet<br>M – total points, $M_a$ – 80% training data, $M_b$ – 20% testing data | | |
|---|---|---|---|
| | No. of Data Points | Pts. Identified by SVM | % Accuracy |
| M | 750 | 658 | 87.7 |
| $M_a$ | 600 | 530 | 88.3 |
| $M_b$ | 150 | 128 | 85.3 |

Table 5: Accuracy of the proposed SVM model based on the bell-mouth training data

| | Bell-mouth Inlet<br>M – total points, $M_a$ – 80% training data, $M_b$ – 20% testing data | | |
|---|---|---|---|
| | No. of Data Points | Pts. Identified by SVM | % Accuracy |
| M | 593 | 519 | 87.5 |
| $M_a$ | 474 | 418 | 88.2 |
| $M_b$ | 119 | 101 | 84.8 |

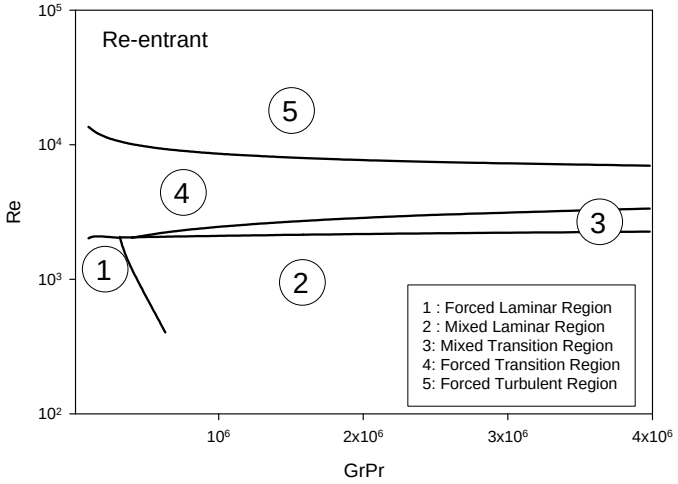


Figure 11: The SVM flow regime map developed by the re-entrant data.

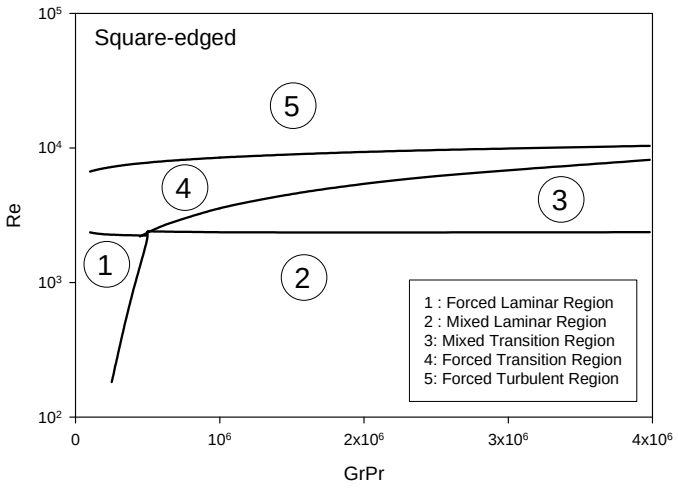


Figure 12: The SVM flow regime map developed by the square-edged data.

## CONCLUSIONS

In this study, the multi-classification SVM model was used to develop new flow regime maps for single-phase forced-mixed convection in horizontal pipes under uniform wall heat flux boundary condition and three different inlet configurations (re-entrant, square-edged, bell-mouth). The results showed that the SVM based flow regime map classified majority of data points (almost 88%) into the correct classes. The overall accuracy of the proposed flow regime map is better than that of Ghajar and Tam (1995). In addition, the prediction of the flow regime boundaries has been improved using the SVM method. Our future plan is to develop a unified map for all three inlet configurations using the SVM method.

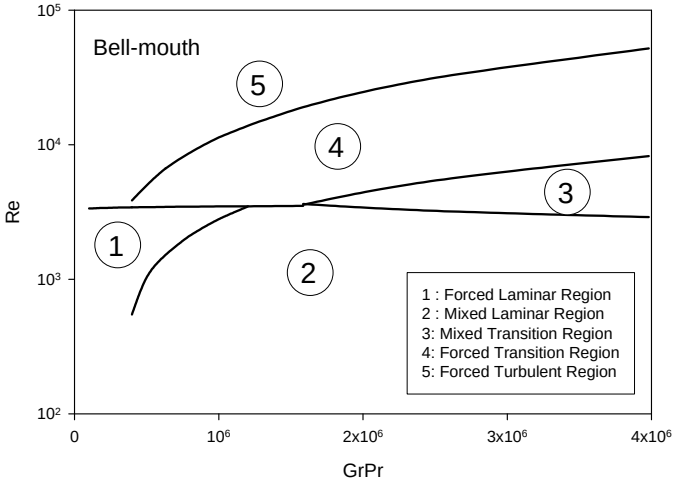


Figure 13: The SVM flow regime map developed by the bell-mouth data.

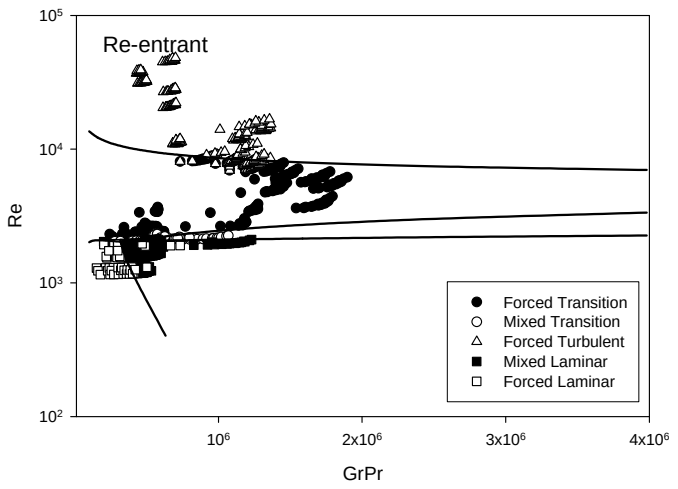


Figure 14: Comparison of proposed SVM flow regime map with the experimental data (Ghajar and Tam, 1994; Tam, 1995) for uniform wall heat flux boundary condition and re-entrant inlet.

## REFERENCES

Aung, W., 1987, "Mixed Convection in Internal Flow," in Handbook of Single-Phase Convective Heat Transfer, S. Kakaç, R. K. Shah, and W. Aung, Eds., Chap. 15, pp. 15-5, Wiley-Interscience, New York.

Boyd, S. and Vandenberghe, L., 2004, "Convex Optimization," Cambridge University Press, New York.

Cortes, C. and Vapnik, V., 1995, "Support Vector Networks," Machine Learning, Vol. 20, pp. 273-297.

Friedman, J., 1996, "Another Approach to Polychotomous Classification," Technical Report, Department of Statistics, Stanford University, Palo Alto, California.

 

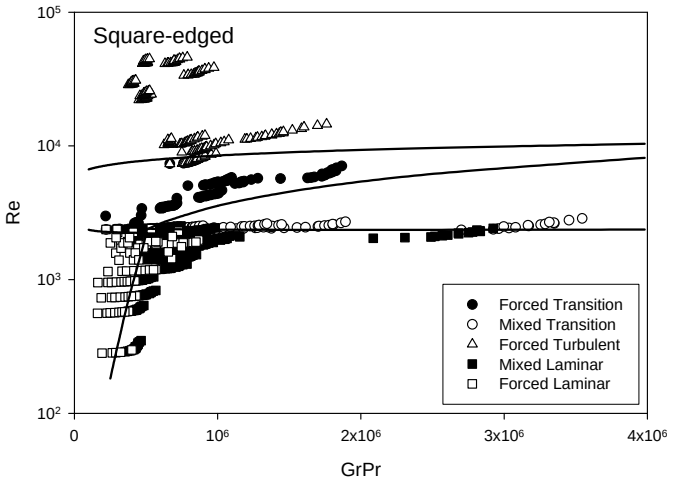


Figure 15: Comparison of proposed SVM flow regime map with the experimental data (Ghajar and Tam, 1994; Tam, 1995) for uniform wall heat flux boundary condition and square-edged inlet.

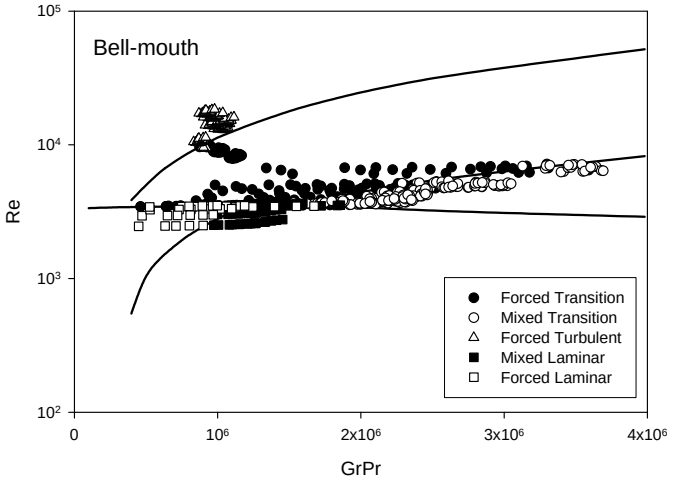


Figure 16: Comparison of proposed SVM flow regime map with the experimental data (Ghajar and Tam, 1994; Tam, 1995) for uniform wall heat flux boundary condition and bell-mouth inlet.

Ghajar, A. J. and Tam, L. M., 1994, "Heat Transfer Measurements and Correlations in the Transition Region for a Circular Tube with Three Different Inlet Configurations," Experimental Thermal and Fluid Science," Vol. 8, No. 1, pp. 79-90.

Ghajar, A. J. and Tam, L. M., 1995, "Flow Regime Map for a Horizontal Pipe with Uniform Heat Flux and Three Different Inlet Configurations," Experimental Thermal and Fluid Science, Vol. 10, No. 3, pp. 287-297.

Ghajar, A. J. and Kim, J., 2006, "Calculation of Local Inside-Wall Convective Heat Transfer Parameters from Measurements of the Local Outside-Wall Temperatures along an Electrically Heated Circular Tube," Heat Transfer Calculations, edited by Myer Kutz, McGraw-Hill, New York, NY, pp. 23.3-23.27.

Hsu, C. W., Lin, C. J., 2002, "A Comparison of Methods for Multi-class Support Vector Machines," IEEE Trans. Neural Networks, Vol. 13, pp.415-425.

Knerr, S., Personnaz, L., and Dreyfus, G., 1990, "Single-Layer Learning Revisited: A Stepwise Procedure for Building and Training a Neural Network." In J. Fogelman, editor, Neurocomputing: Algorithms, Architectures and Applications. Springer-Verlag, New York.

Kern, D. Q., and Othmer, D. F., 1943, "Effect of Free Convection on Viscous Heat Transfer in Horizontal Tubes," AICHE J., Vol. 39, pp. 517-555.

Metais, B., 1963, "Criteria for Mixed Convection," HTL Tech. Rep. No. 51, Heat Transfer Laboratory, Univ. Minnesota, Minneapolis, MN.

Metais, B., and Eckert, E. R. G., 1964, "Forced, Mixed and Free Convection Regimes," J. Heat Transfer, Vol. 86, pp. 295-296.

Schölkopf, B. and Smola, A. J., 2002, "Learning with Kernels – Support Vector Machines, Regularization, Optimization and Beyond," MIT Press, Cambridge, MA.

Tam, L. M., 1995, "An Experimental Investigation of Heat Transfer and Pressure Drop in the Transition Region for a Horizontal Tube with Different Inlets and Uniform Wall Heat Flux", PhD. dissertation, Oklahoma State University, Stillwater, Oklahoma.

Tam, L. M., and Ghajar, A. J., 1998, "The Unusual Behavior of Local Heat Transfer Coefficient in a Circular Tube with a Bell-Mouth Inlet," Experimental Thermal and Fluid Science, vol. 16, pp. 187–194.

Tam, L. M., and Ghajar, A. J., 2006, "Transitional Heat Transfer in Plain Horizontal Tubes," Heat Transfer Engineering, Vol. 27, No. 5, pp 23-38.

Trafalis, T. B., Oladunni, O., and Papavassiliou, D. V., 2005, "Two-phase Flow Regime Identification with a Multiclassification Support Vector Machine (SVM) Model," Industrial and Engineering Chemistry Research, Vol. 44, No.12, pp. 4414-4426.

Vapnik, V., 1979, "Estimation of Dependencies Based on Empirical Data (in Russian)," Nauka, Moscow, (English translation: Vladimir Vapnik (1982), Estimation of Dependencies Based on Empirical Data, Springer, New York.)

Vapnik, V., 1995, "The Nature of Statistical Learning Theory," Springer-Verlag, New York.

 